Bedforms in a turbulent stream: ripples, chevrons and antidunes — Online Supplementary Material —

By BRUNO ANDREOTTI, PHILIPPE CLAUDIN, OLIVIER DEVAUCHELLE, ORENCIO DURÁN AND ANTOINE FOURRIÈRE

Laboratoire de Physique et Mécanique des Milieux Hétérogènes, PMMH UMR 7636 ESPCI – CNRS – Univ. Paris Diderot, 10 rue Vauquelin, 75005, Paris, France

(Received 7 September 2011)

In this supplementary part, we formulate the technical framework of the Reynolds averaged hydrodynamical description of a turbulent flow over a wavy bottom that we use in the main paper. We also relate it to a simplified depth averaged description. Through linearising the equations in the limit of bedforms of vanishing amplitude, we determine the different regimes and the dominant dynamical mechanisms at work in each of them. finally, the role of secondary parameters in the bifurcation diagram for antidunes is shown.

1. Hydrodynamical descriptions

1.1. *Reynolds averaged description*

We consider a turbulent flow over a wavy bed. Following Reynolds' decomposition between average and fluctuating (denoted with a prime) quantities, the equations governing the mean velocity field u_i can be written as:

$$\partial_i u_i = 0, \tag{1.1}$$

$$D_t u_i = \partial_t u_i + u_j \partial_j u_i = -\partial_j \tau_{ij} - \partial_i p, \tag{1.2}$$

where p is the pressure and $\tau_{ij} = \overline{u_i' u_j'}$ is the Reynolds stress tensor (Reynolds 1874). The density factor ρ is taken as unit. We use the same description of turbulence over a relief as in Fourrière et al. 2010. The anisotropy of the Reynolds stress and the lag between the shear rate and the resulting turbulent stress can be neglected. Introducing the strain rate tensor $\dot\gamma_{ij} = \partial_i u_j + \partial_j u_i$ and its squared modulus $|\dot\gamma|^2 = \frac{1}{2}\dot\gamma_{ij}\dot\gamma_{ij}$, the Reynolds stress τ_{ij} is expressed in a tensorial form:

$$\tau_{ij} = \kappa^2 L^2 |\dot\gamma| \left(\frac{1}{3}\chi^2 |\dot\gamma|\, \delta_{ij} - \dot\gamma_{ij} \right), \tag{1.3}$$

where $\kappa \simeq 0.4$ is the von Kármán constant and χ another phenomenological constant associated to normal stresses.

Considering a homogeneous river of depth H inclined at an angle θ to the horizontal, the shear stress τ_{xz} must balance gravity. It thus varies linearly as $\tau_{xz} = g(z-H)\sin\theta$ and vanishes at the free surface. By definition of the shear velocity u_*, we also write $\tau_{xz} \equiv u_*^2(z/H - 1)$. The mixing length is chosen equal to $L = (z + z_0)\sqrt{1 - z/H}$, where

z_0 is the hydrodynamical roughness. This choice results into a logarithmic base flow, consistently with field and experimental observations:

$$u_x = \frac{u_*}{\kappa} \ln\left(1 + \frac{z}{z_0}\right). \tag{1.4}$$

The stress balance equation along the z-axis allows to get the pressure, which reads:

$$p + \tau_{zz} = p_0 + g(H - z)\cos\theta = p_0 + \frac{u_*^2}{\tan\theta}\left(1 - \frac{z}{H}\right). \tag{1.5}$$

We define the surface Froude number as the ratio of the surface velocity to the velocity of gravity surface waves (in the case of a flat bottom):

$$\mathcal{F} \equiv \frac{1}{\sqrt{gH}} \frac{u_*}{\kappa} \ln\left(1 + \frac{H}{z_0}\right) = \frac{1}{\kappa} \ln\left(1 + \frac{H}{z_0}\right) \sqrt{\sin\theta}. \tag{1.6}$$

The Froude number can be of order 1 in flumes but is in general small for large natural rivers, due to their small slopes.

We now consider a wavy bottom of the form $Z = \zeta e^{ik(\cos\alpha\ x + \sin\alpha\ y)}$. We wish to perform the linear expansion of the equations with respect to the small parameter $k\zeta$. We note $\eta = kz$, $\eta_0 = kz_0$ and $\eta_H = kH$. We write the first order corrections to the base flow as

$$u_x = u_* \left[\mu + kZU\right], \tag{1.7}$$

$$u_y = u_* kZV, \tag{1.8}$$

$$u_z = u_* kZW, \tag{1.9}$$

$$\tau_{xz} = \tau_{zx} = -u_*^2 \left[1 - \frac{\eta}{\eta_H} + kZS_{xz}\right], \tag{1.10}$$

$$\tau_{yz} = \tau_{zy} = -u_*^2 \left[kZS_{yz}\right], \tag{1.11}$$

$$\tau_{xy} = \tau_{yx} = -u_*^2 \left[kZS_{xy}\right], \tag{1.12}$$

$$p + \tau_{zz} = p_0 + u_*^2 \left[\frac{1}{\tan\theta}\left(1 - \frac{\eta}{\eta_H}\right) + kZS_n\right], \tag{1.13}$$

$$\tau_{xx} = u_*^2 \left[\frac{1}{3}\chi^2 + kZS_{xx}\right], \tag{1.14}$$

$$\tau_{yy} = u_*^2 \left[\frac{1}{3}\chi^2 + kZS_{yy}\right], \tag{1.15}$$

$$\tau_{zz} = u_*^2 \left[\frac{1}{3}\chi^2 + kZS_{zz}\right], \tag{1.16}$$

where the function μ is defined by $\mu(\eta) = \frac{1}{\kappa}\ln\left(\frac{\eta}{\eta_0}\right)$. The quantities U, W, etc, are functions of η. The free surface is also perturbed and we denote $h = H + \Delta(x, y)$ the flow depth at the position x, y. The modified expression for the mixing length then reads

$$L = (z_0 + z - Z)\sqrt{\frac{H + \Delta - z}{H + \Delta - Z}}. \tag{1.17}$$

In the following, we write the free surface profile as $\Delta = \delta Z$.

At the linear order, the stress equations can be simplified into

$$\mu' S_{xz} = 2\left(1 - \frac{\eta}{\eta_H}\right)\left((U' + i\cos\alpha\ W) - \kappa\mu'^2 + \frac{\mu'}{2\eta_H} + \frac{\eta\delta\mu'}{2\eta_H^2\left(1 - \frac{\eta}{\eta_H}\right)}\right), \tag{1.18}$$

$$\mu' S_{xy} = \left(1 - \frac{\eta}{\eta_H}\right)(i \sin\alpha\ U + i\cos\alpha\ V)\,, \tag{1.19}$$

$$\mu' S_{yz} = \left(1 - \frac{\eta}{\eta_H}\right)(V' + i\sin\alpha\ W)\,, \tag{1.20}$$

$$\mu'(S_{xx} - S_{zz}) = \left(1 - \frac{\eta}{\eta_H}\right)(-2i\cos\alpha\ U + 2W')\,, \tag{1.21}$$

$$\mu'(S_{yy} - S_{zz}) = \left(1 - \frac{\eta}{\eta_H}\right)(-2i\sin\alpha\ V + 2W')\,, \tag{1.22}$$

$$\tag{1.23}$$

which give the following two equations:

$$U' = -i\cos\alpha\ W + \frac{\mu' S_{xz}}{2\left(1 - \frac{\eta}{\eta_H}\right)} + \kappa\mu'^2 - \frac{\mu'}{2\eta_H} - \delta\,\frac{\eta\mu'}{2\eta_H^2\left(1 - \frac{\eta}{\eta_H}\right)}\,, \tag{1.24}$$

$$V' = -i\sin\alpha\ W + \frac{\mu' S_{yz}}{\left(1 - \frac{\eta}{\eta_H}\right)}\,. \tag{1.25}$$

The Navier-Stokes equations lead to

$$W' = -i\cos\alpha\ U - i\sin\alpha\ V, \tag{1.26}$$

$$S'_{xz} = i\mu\cos\alpha\ U + \mu' W + i\cos\alpha\ (S_n + S_{xx} - S_{zz}) - i\sin\alpha\ S_{xy} \tag{1.27}$$

$$= i\mu\cos\alpha\ U + \mu' W + i\cos\alpha\ S_n + \frac{\left(1 - \frac{\eta}{\eta_H}\right)}{\mu'}\left[(1 + 3\cos^2\alpha)\ U + 3\sin\alpha\ \cos\alpha\ V\right],$$

$$S'_{yz} = i\mu\cos\alpha\ V + i\sin\alpha\ (S_n + S_{yy} - S_{zz}) - i\cos\alpha\ S_{yx} \tag{1.28}$$

$$= i\mu\cos\alpha\ V + i\sin\alpha\ S_n + \frac{\left(1 - \frac{\eta}{\eta_H}\right)}{\mu'}\left[3\sin\alpha\cos\alpha\ U + (1 + 3\sin^2\alpha)\ V\right],$$

$$S'_n = -i\mu\cos\alpha\ W + i\cos\alpha\ S_{xz} + i\sin\alpha\ S_{yz}. \tag{1.29}$$

Introducing the vector $\vec{X} = (U, V, W, S_{xz}, S_{yz}, S_n)$, at the first order in $k\zeta$, one has to solve a closed system of six differential equations which can be written under the following form:

$$\frac{d}{d\eta}\vec{X} = \mathcal{P}\vec{X} + \vec{S} + \delta\vec{S_\delta}, \tag{1.30}$$

with

$$\mathcal{P} = \begin{pmatrix} 0 & 0 & -i\cos\alpha & \frac{\mu'}{2\left(1-\frac{\eta}{\eta_H}\right)} & 0 & 0 \\ 0 & 0 & -i\sin\alpha & 0 & \frac{\mu'}{\left(1-\frac{\eta}{\eta_H}\right)} & 0 \\ -i\cos\alpha & -i\sin\alpha & 0 & 0 & 0 & 0 \\ \frac{1+3\cos^2\alpha}{\mu'}\left(1-\frac{\eta}{\eta_H}\right) + i\mu\cos\alpha & \frac{3\sin\alpha\cos\alpha}{\mu'}\left(1-\frac{\eta}{\eta_H}\right) & \mu' & 0 & 0 & i\cos\alpha \\ \frac{3\sin\alpha\cos\alpha}{\mu'}\left(1-\frac{\eta}{\eta_H}\right) & \frac{1+3\sin^2\alpha}{\mu'}\left(1-\frac{\eta}{\eta_H}\right) + i\mu\cos\alpha & 0 & 0 & 0 & i\sin\alpha \\ 0 & 0 & -i\mu\cos\alpha & i\cos\alpha & i\sin\alpha & 0 \end{pmatrix}, \tag{1.31}$$

$$\vec{S} = \begin{pmatrix} \kappa\mu'^2 - \frac{\mu'}{2\eta_H} \\ 0 \\ 0 \\ 0 \\ 0 \\ 0 \end{pmatrix}, \quad \text{and} \quad \vec{S_\delta} = \begin{pmatrix} -\frac{\eta\mu'}{2\eta_H^2\left(1-\frac{\eta}{\eta_H}\right)} \\ 0 \\ 0 \\ 0 \\ 0 \\ 0 \end{pmatrix}. \tag{1.31}$$

The boundary conditions are the following: the velocity vanishes on the bed; the particles cannot cross the free surface; the shear and normal stesses vanish at the free surface. Making use of the linearity of the equations, we seek the solution under the form $\vec{X} = \vec{X}_0 + a_{xz}\vec{X}_{xz} + a_{yz}\vec{X}_{yz} + a_n\vec{X}_n + \delta\vec{X}_\delta$, where the vectors $\vec{X}_0$, $\vec{X}_{xz}$, $\vec{X}_{yz}$, $\vec{X}_n$ and $\vec{X}_\delta$ are solutions of the equations:

$$\frac{d}{d\eta}\vec{X}_s = \mathcal{P}\vec{X}_s + \vec{S} \qquad \text{with} \qquad \vec{X}_s(0) = \begin{pmatrix} -1/(\kappa\eta_0) \\ 0 \\ 0 \\ 0 \\ 0 \\ 0 \end{pmatrix}, \tag{1.32}$$

$$\frac{d}{d\eta}\vec{X}_{xz} = \mathcal{P}\vec{X}_{xz} \qquad \text{with} \qquad \vec{X}_{xz}(0) = \begin{pmatrix} 0 \\ 0 \\ 0 \\ 1 \\ 0 \\ 0 \end{pmatrix}, \tag{1.33}$$

$$\frac{d}{d\eta}\vec{X}_{yz} = \mathcal{P}\vec{X}_{yz} \qquad \text{with} \qquad \vec{X}_{yz}(0) = \begin{pmatrix} 0 \\ 0 \\ 0 \\ 0 \\ 1 \\ 0 \end{pmatrix}, \tag{1.34}$$

$$\frac{d}{d\eta}\vec{X}_n = \mathcal{P}\vec{X}_n \qquad \text{with} \qquad \vec{X}_n(0) = \begin{pmatrix} 0 \\ 0 \\ 0 \\ 0 \\ 0 \\ 1 \end{pmatrix}. \tag{1.35}$$

$$\frac{d}{d\eta}\vec{X}_\delta = \mathcal{P}\vec{X}_\delta + \vec{S}_\delta \qquad \text{with} \qquad \vec{X}_\delta(0) = \begin{pmatrix} 0 \\ 0 \\ 0 \\ 0 \\ 0 \\ 0 \end{pmatrix}. \tag{1.36}$$

The bottom boundary conditions $U(0) = -1/(\kappa\eta_0)$, $V(0) = 0$ and $W(0) = 0$ are then automatically satisfied. At the free surface, we impose the material nature of the surface, $W(\eta_H) = i\mu(\eta_H)\cos\alpha\,\delta$, and vanishing stresses: $S_{xz}(\eta_H) = \delta/\eta_H$, $S_{yz}(\eta_H) = 0$ and $S_n(\eta_H) = \delta/(\eta_H\,\tan\theta)$. These last four conditions select the coefficients a_{xz}, a_{yz} and a_n as well as the value of δ.

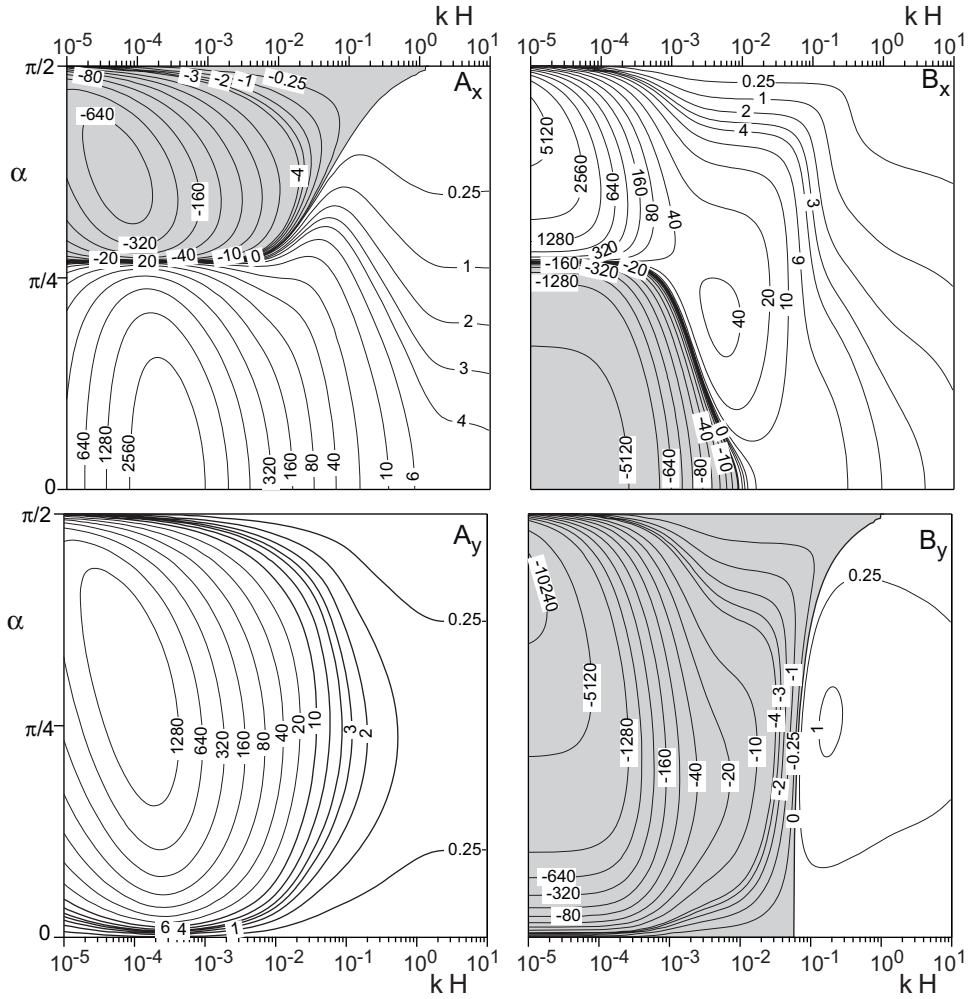

FIGURE 1. Basal shear stresses A_x, B_x, A_y, B_y as functions of kH and α for $H/z_0 = 10^2$ and $\mathcal{F} = 0.1$.

We focus on the stress components on the bed and define the coefficients A_x, B_x, A_y and B_y as:

$$S_{xz}(0) = A_x + iB_x, \tag{1.37}$$

$$S_{yz}(0) = A_y + iB_y, \tag{1.38}$$

Integration of equation (1.31) yields to the variations of these stress coefficients with k and α (Fig. 1).

1.2. *Description à la Saint-Venant*

In the limit of vanishing kH, one expects a simplified depth averaged (Saint-Venant) description to be valid. We consider the Saint-Venant equations without source terms. The continuity and momentum equations read:

$$\vec{\nabla} \cdot (h\vec{u}) = 0, \tag{1.39}$$

$$\vec{u} \cdot \vec{\nabla}\vec{u} = -g\vec{\nabla}(Z + h) - C\,\frac{|\vec{u}|\,\vec{u}}{h}. \tag{1.40}$$

To relate Saint-Venant to the Reynolds average model, we define the Chezy coefficient:

$$C = \frac{\overline{u}^2}{u_*^2} \simeq \left(\frac{\kappa}{\ln\left(1 + H/z_0\right) - 1} \right)^2 . \tag{1.41}$$

For H/z_0 in the range 10^3–10^4, C is on the order of few 10^{-3}. One can normalise vertical lengths Z and h by the flow depth H, the velocity u by its average $\overline{u}$, horizontal lengths x and y by H/C and the time t by a transport time-scale. Then, there remains a single non-dimensional parameter in the flow equations, the Froude number $\mathcal{F} = \overline{u}/\sqrt{gH}$. Contrarily to the Reynolds averaged description, the scaling laws with respect to the ratio H/z_0 can thus be deduced from dimensional analysis.

Considernig as before a wavy bottom $Z = \zeta e^{ik(\cos\alpha\ x + \sin\alpha\ y)}$, we perform the linear expansion with respect to the small parameter $k\zeta$ around the base state $h = H$ and $\vec{u} = \overline{u}\vec{e}_x$:

$$h = H + \Delta, \tag{1.42}$$

$$\vec{u} = \overline{u}\vec{e}_x + u_\parallel \vec{e}_\parallel + u_\perp \vec{e}_\perp, \tag{1.43}$$

where we have decomposed the velocity disturbance along the directions parallel and transverse to the crests:

$$\vec{e}_\parallel = -\sin\alpha\, \vec{e}_x + \cos\alpha\, \vec{e}_y, \tag{1.44}$$

$$\vec{e}_\perp = \cos\alpha\, \vec{e}_x + \sin\alpha\, \vec{e}_y. \tag{1.45}$$

The linearised Saint-Venant equations then become:

$$\frac{u_\perp}{\overline{u}} = -\cos\alpha\, \frac{\Delta}{H} \tag{1.46}$$

$$ikH\, \cos\alpha\, \frac{u_\parallel}{\overline{u}} + C\left[\left(1 + \sin^2\alpha\right) \frac{u_\parallel}{\overline{u}} - \sin\alpha\cos\alpha \frac{u_\perp}{\overline{u}} + \sin\alpha \frac{\Delta}{H} \right] = 0 \tag{1.47}$$

$$ikH\, \cos\alpha\, \frac{u_\perp}{\overline{u}} + C\left[\left(1 + \cos^2\alpha\right) \frac{u_\perp}{\overline{u}} - \sin\alpha\cos\alpha \frac{u_\parallel}{\overline{u}} - \cos\alpha \frac{\Delta}{H} \right] + \frac{ik}{\mathcal{F}^2}\left(Z + \Delta\right) = 0 \tag{1.48}$$

The conservation of mass directly relates the transverse velocity to the flow depth modulation. Along the direction parallel to the crest, there is a balance between inertia and friction. Due to the invariance in that direction, there is no gravity effect in this momentum balance. By contrast, along the direction normal to the crest, the balance is between inertia, friction, and two different gravity terms (terms scaling as $1/\mathcal{F}^2$): the component of gravity proportional to the slope and the gravity induced pressure gradient, proportional to the flow thickness gradient.

The shear stress is not part of the variables of this modeling, but we can consistently define it as $\vec{\tau} = -C|\vec{u}|\vec{u}$. The basal shear stress coefficients are then related to the velocity disturbance as:

$$A_x + iB_x = \frac{2}{C\, kZ_1} \left(\cos\alpha\, \frac{u_\perp}{\overline{u}} - \sin\alpha\, \frac{u_\parallel}{\overline{u}} \right) \tag{1.49}$$

$$A_y + iB_y = \frac{1}{C\, kZ_1} \left(\sin\alpha\, \frac{u_\perp}{\overline{u}} + \cos\alpha\, \frac{u_\parallel}{\overline{u}} \right) \tag{1.50}$$

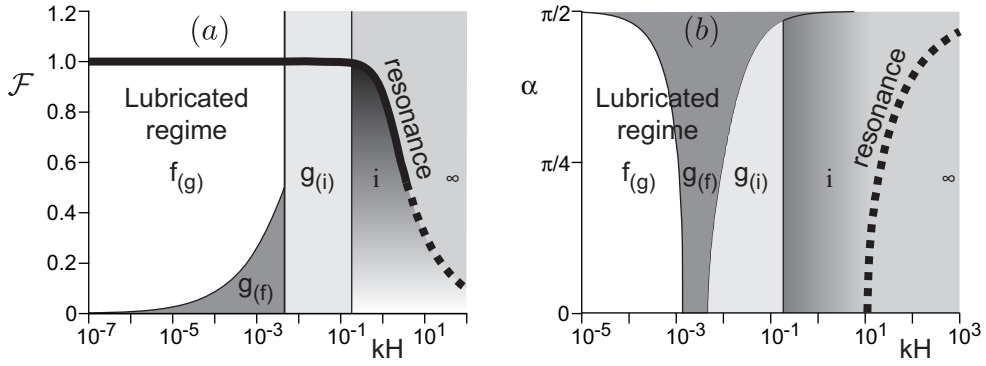

FIGURE 2. Regime diagram. (a) Diagram in the plane $\mathcal{F}$ vs kH, for the angle $\alpha = 0$. (b) Diagram in the plane α vs kH, for $\mathcal{F} = 0.3$. The line thick line is the resonance curve (Eq. 2.5) – we display it dashed when the relative resonance amplitude is so small that the stress component B_x remains positive. For the names of the different regimes, see section titles.

Introducing a rescaled wave-number $\tilde{k} = kH/C$, these coefficients read:

$$A_x + iB_x = \frac{2\cos\alpha\,(i - \tilde{k}\cos\alpha - i\tan^2\alpha)}{C(\tilde{k}\cos\alpha - i)\Big[(\mathcal{F}^2-1)\,\tilde{k}\cos\alpha - 3i\mathcal{F}^2\Big] - \tilde{k}\sin\alpha\tan\alpha(\tilde{k}\cos\alpha - 2i)}\,, \quad (1.51)$$

$$A_y + iB_y = \frac{\sin\alpha\,(-\tilde{k}\cos\alpha + 3i)}{C(\tilde{k}\cos\alpha - i)\Big[(\mathcal{F}^2-1)\,\tilde{k}\cos\alpha - 3i\mathcal{F}^2\Big] - \tilde{k}\sin\alpha\tan\alpha(\tilde{k}\cos\alpha - 2i)}\,. \quad (1.52)$$

2. Linear response of the basal shear stress to the presence of bedforms

As the result of the integration of the above linearised equations, we identify in this section the different hydrodynamical regimes of a flow over a wavy bottom $Z = \zeta e^{ik(\cos\alpha\, x + \sin\alpha\, y)}$, for which $k\zeta \ll 1$. As shown below, these regimes can be represented in the plane $(\mathcal{F}, kH)$ for a given beform angle α, or in the plane (α, kH) for a given Froude number $\mathcal{F}$, see figure 2.

2.1. *The unbounded limit (regime ∞)*

We consider the limit of bedforms whose wavelength is much smaller than the flow thickness: $kH \gg 1$. We first consider the case of transverse bedforms, detailled in Fourrière et al. 2010. As shown by Jackson & Hunt (1975), the turbulent flow over such a wavy bottom can be decomposed into three regions.

• *Outer layer* – In the outer layer, away from the bottom, the pressure gradient is mostly balanced by inertial terms, like in an inviscid potential flow. The streamlines follow the topography so that the velocity at the bottom of the outer layer is in phase with the bottom.

• *Inner layer* – In the inner layer, the inertial terms of the Navier-Stokes equation are negligible, and the longitudinal pressure gradient is thus balanced by the Reynolds shear stress transverse gradient i.e. by the mixing of momentum due to turbulent fluctuations. The thickness ℓ of the inner layer is related to wavelength by $\lambda \sim \ell \ln^2(\ell/z_0)$. At the transition between the inner and outer layers, the fluid velocity is slowed down by the shear stress. In the limit of a small aspect ratio $k\zeta$, the velocity, which is inherited from the outer layer, is always phase delayed with respect to the shear stress.: when a stress is

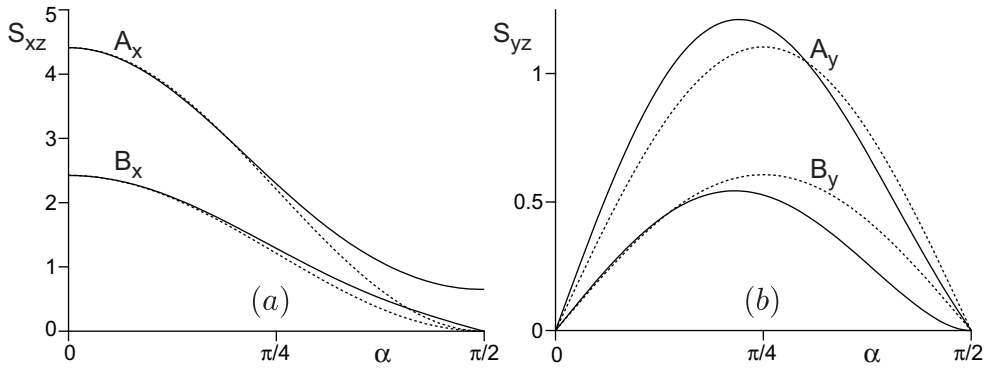

FIGURE 3. Dependence of the basal shear stresses on the bedform angle α in the unbounded regime (regime ∞). Solid line: computation for $\eta_0 = 10$ and for asymptotically large kH. Dotted lines: equations (2.1-2.4). (a) Longitudinal shear stress coefficients A_x and B_x. (b) Transverse shear stress coefficients A_y and B_y.

applied, the velocity response is lagged, due to inertia. As a consequence, the shear stress is phase-advanced with respect to the topography, which means that the shear stress reaches its maximum upstream of the crests of the bumps. The shear stress phase shift B_x/A_x vanishes for asymptotically small kz_0 and gently increases with $\ln(kz_0)$ (see figures in Fourrière et al. 2010). The asymptotic calculation performed by Jackson & Hunt 1975 and simplified by Kroy et al. 2002 is recovered but only for asymptotically large $\ln(\lambda/z_0)$, a limit hardly reached in real problems.

• *Surface layer* – The surface layer, of thickness h_0, is responsible for the hydrodynamical roughness z_0 seen from the inner layer. The dominant physical mechanism at work in this surface layer can be of different nature. For instance, z_0 can result from the mixing due to roughness elements, the predominance of viscous dissipation, or the presence of bed-load transport. The shear stress profile is insensitive to the mechanisms at work in the surface layer, provided that its thickness h_0 is smaller than the inner layer thickness ℓ: the hydrodynamical roughness z_0 is then the single quantity inherited from the surface layer.

We can now analyse the dependence of the shear stress coefficients on the angle α. For an asymptotically small value of η_0, one expects the basal shear stress to be directly governed by the velocity at the bottom of the outer layer. In the latter, the pressure field is solution of the Laplace equation so that all disturbance fields decrease exponentially as $\exp(-\eta)$. At the linear order, the pressure gradient is balanced by the longitudinal inertia: $\bar{u}\,\partial_x u_i \simeq -\partial_i p$, where $\bar{u}$ is the mean velocity in the outer layer. The planar velocity disturbance is thus normal to the crest and in phase with the relief. As the sand bed is a material surface, the vertical velocity is proportional to the longitudinal bed slope: $u_z = i\overline{u}\,\cos\alpha\, kZ\, \exp(-\eta)$ and is thus proportional to $\cos\alpha$. The longitudinal velocity component u_x thus goes like $\cos^2\alpha$ and the transverse one like $\sin\alpha\cos\alpha$. On the bed, this would result into shear stress coefficients scaling as:

$$A_x(\alpha) = A_x(0)\,\cos^2\alpha, \tag{2.1}$$

$$B_x(\alpha) = B_x(0)\,\cos^2, \alpha, \tag{2.2}$$

$$A_y(\alpha) = \frac{1}{2}\,A_x(0)\,\cos\alpha\sin\alpha, \tag{2.3}$$

$$B_y(\alpha) = \frac{1}{2}\,B_x(0)\,\cos\alpha\sin\alpha. \tag{2.4}$$

Note that the factor 1/2 in the transverse direction comes from the scaling of the shear stress as the square of the velocity. In figure 3, we compare these predictions to the numerical integration of the linear equations. One observes that the main trends are captured by the above expressions, but that there remain significant discrepancies. In particular, the longitudinal velocity remains modulated ($A_x \neq 0$), even for purely longitudinal patterns (for $\alpha \to \pi/2$).

2.2. *Resonance of standing waves*

We now consider bedforms whose wavelength λ is large enough to be influenced by the free surface. The hydrodynamical behaviour depends both on the Froude number $\mathcal{F}$ and on the wavenumber rescaled by the flow depth, kH. The undulations of the bottom excite standing gravity waves at the free surface. Recall that we note $H + \Delta$ the flow depth, and define $\delta = |\delta| e^{i\varphi} = \Delta/Z$. Resonant conditions are reached when these waves propagate at a velocity equal to the flow velocity component along the direction normal to the crest, i.e. when

$$\mathcal{F}^2 \simeq \frac{\tanh(kH)}{kH \cos^2 \alpha} \tag{2.5}$$

Along the resonant curve, inertial effects and gravity are on the same order. Figure 4a shows the amplitude of deformation of the free surface predicted by the model. One observes that equation (2.5) correctly predicts the qualitative behavior, i.e. the approximative location of the surface modulation maxima in the plane (α, kH). The discrepancy comes from the definition of the Froude number, based on the surface velocity. In reality, the resonance involves a region close to the surface, of thickness $\mathcal{O}(\lambda)$, on which the velocity should be averaged.

Standing gravity waves excited at the free surface by the bedforms are in phase at small λ/H (supercritical regime) and in antiphase at large λ/H (subcritical regime). In between, at the resonance, the response of the free surface is in quadrature with the disturbance (Fig. 4b) so that, in the outer layer, the streamlines are squeezed downstream of the crests of the bump. Around the free surface resonance, the velocity at the bottom of the outer layer is thus phase-delayed with respect to the topography. However, the basal shear stress is phase-advanced with respect to this velocity. When the Froude number $\mathcal{F}$ is large enough, the deformation of the free surface is so large that it has a dominant effect on the flow close to the bottom and the phase shift B/A between the shear stress and the topography becomes negative (Fig. 4d,f). Conversely, at small $\mathcal{F}$, the free surface deformation does not influence enough the flow close to the bottom and B/A remains positive.

2.3. *Cross-over between the resonance and the shallow water limit (regime i)*

Between the shallow water region ($kH \ll 1$) and the resonance band ($\mathcal{F}^2 \simeq \tanh(kH)/(kH)$), the free surface is in antiphase with the topography and has a very small modulation amplitude. Thus, the velocity at the bottom of the outer layer is in phase with the topography. Due to the confinement, the velocity increases at the top of the bumps. From the conservation of flow rate, one can infer that, in the limit of small kH, the velocity disturbance in the inner layer is proportional to $\overline{u}\zeta/H$. As the shear stress is quadratic in u_x, one expects a scaling law of the form $A_x(\alpha = 0) \simeq \frac{2}{kH}$. Figure 5 shows that this scaling is verified both for a rigid top boundary and for a free surface.

In the limit $kH \ll 1$, the water depth becomes much thinner than the wavelength, and the inner layer invades the whole flow (i.e. $\ell \simeq H$). In the cross-over region between the resonance and the shallow water limit, the transition zone between the outer and inner layers responsible for the upstream shift of the shear stress with respect to the

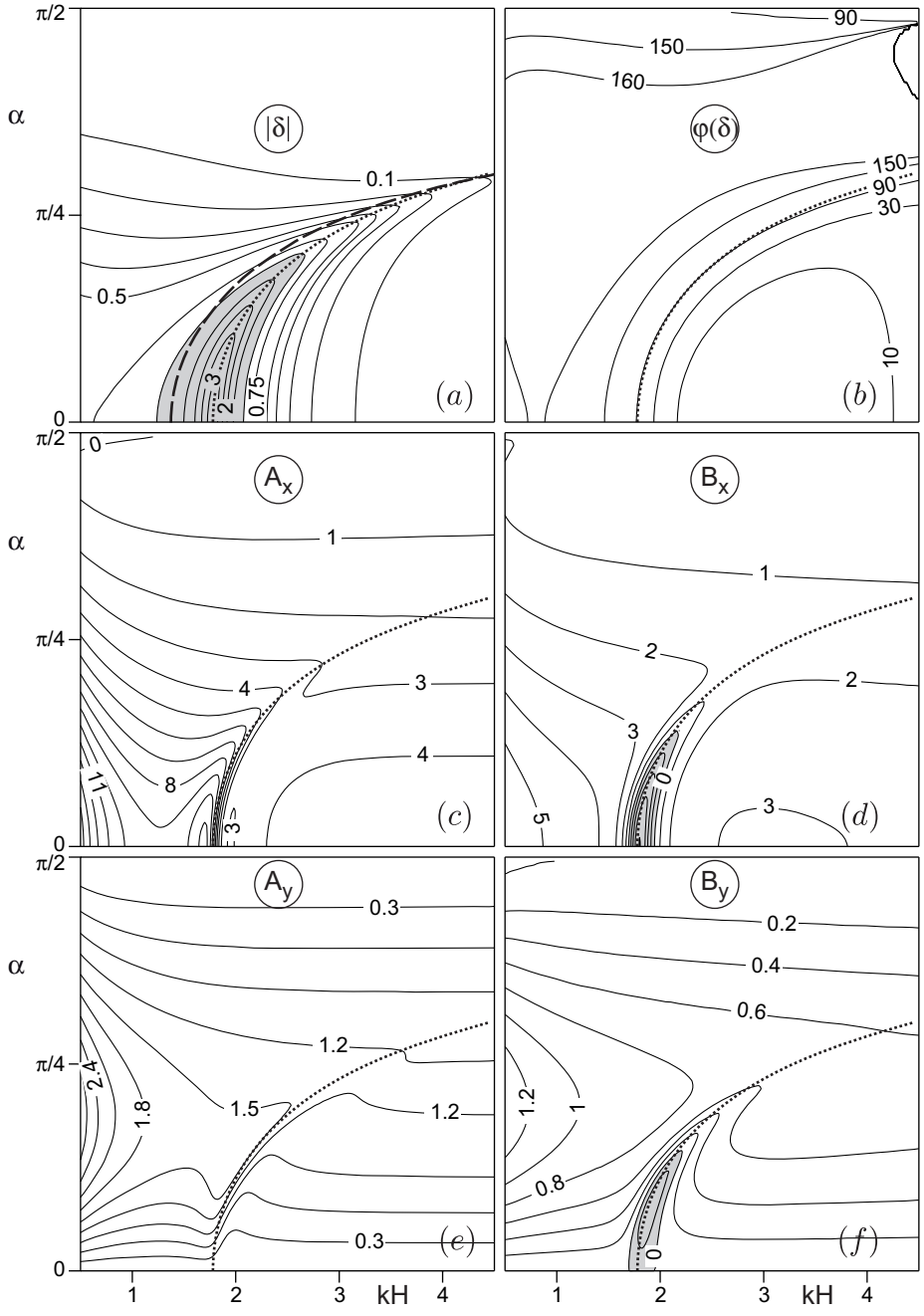

[p]

FIGURE 4. Resonance of the surface standing waves for $H/z_0 = 10^2$ and $\mathcal{F} = 0.8$ (dotted line). (a) Amplitude of the free surface modulation. Contours plotted for $|\delta| = 0.1$, 0.2, 0.3, 0.4, 0.5, 0.75, 1, 1.5, 2, 2.5 and 3. Gray zone: $|\delta| > 1$. The dashed line is the prediction of eq. (2.5). (b) Phase of the free surface modulation. Contours plotted for $\phi(\delta) = 10°$, 30°, 90°, 150°, 160°. (c) Coefficient A_x. Contours plotted from $A_x = 0$ to $A_x = 14$ by increment of 1. (d) Coefficient B_x. Contours plotted from $B_x = -4$ to $B_x = 5$ by increment of 1. Gray zone: $B_x < 0$. (e) Coefficient A_y. Contours plotted from $A_y = 0.3$ to $A_y = 2.7$ by increment of 0.3. (f) Coefficient B_y. Contours plotted from $B_y = -0.2$ to $B_y = 1.2$ by increment of 0.2.

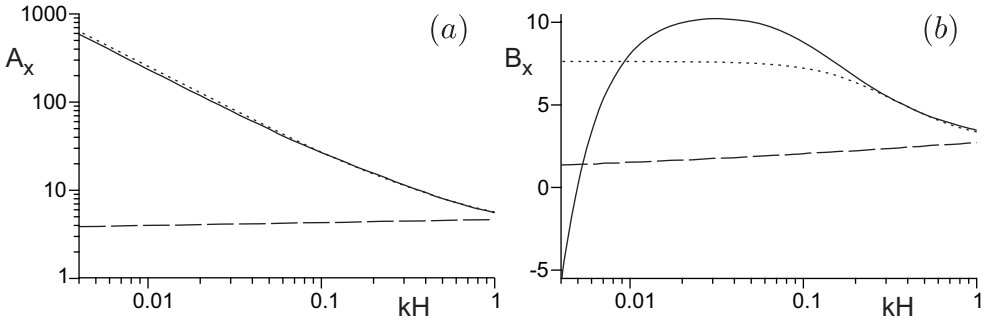

FIGURE 5. Basal shear stresses A_x and B_x as functions of kH in the cross-over regime (regime III). The parameters are $\alpha = 0$, $H/z_0 = 10^2$ and $\mathcal{F} = 0.1$. The free surface situation (solid line) is compared to the unbounded one (dashed line) and to the case of a rigid top boundary (dotted line). The large increase of A_x in this range of wavelength results from the confinement of the flow. Due to inertia, the shear stress is still phase advanced with respect to the topography, although the inner layer becomes comparable to the whole flow thickness.

topography progressively disappears. The phase lag B_x/A_x between the shear stress and the topography thus decreases with kH and becomes negative ($B_x/A_x < 0$) below a threshold value of kH that increases with the Froude number. As A_x is increasing at the same time, B_x passes through a maximum value.

2.4. *The flat free surface regime, with inertia dominating friction (regime $g_{(i)}$)*

Going further in the limit of small kH, one can analyse the last three hydrodynamical regimes within the simpler St-Venant framework, which gives close results to the full model (Fig. 6). We consider here the asymptotic regime where the gravity-induced pressure balances the slope effects ($\mathcal{F} \to 0$), with a negligible friction force ($C \to 0$). Then, from the force balance in the direction normal to the bedforms, one deduces that the free surface is flat, i.e. $\Delta = -Z$. The conservation of mass then leads to $u_\perp = \overline{u} \cos\alpha \, \frac{Z}{H}$. Along the direction parallel to the bedforms, inertia is balanced by friction. In this inertia dominated regime, $u_\parallel$ is null at the leading order, so that:

$$A_x = \frac{2\,\cos^2\alpha}{kH} \quad \text{and} \quad A_y = \frac{\sin\alpha\cos\alpha}{kH} \tag{2.6}$$

Reintroducing the friction force at the perturbative order, one obtains:

$$ikH\,\cos\alpha\,\frac{u_\parallel}{\overline{u}} \sim C\,\sin\alpha\left[\cos\alpha\frac{u_\perp}{\overline{u}} + \frac{Z}{H}\right] \sim C\,\sin\alpha\left(\cos^2\alpha + 1\right)\,\frac{Z}{H} \tag{2.7}$$

The flow velocity is maximal and its thickness minimal on the crests. As a consequence, friction increases. Inertia balances the component of this additional friction parallel to the crest. The velocity component parallel to the crest is thus phase delayed (in quadrature) with respect to friction. This results into a positive B_x and a negative B_y.

$$B_x = \frac{2C\,(\cos^2\alpha + 1)\sin\alpha\,\tan\alpha}{(kH)^2} \quad \text{and} \quad B_y = -\frac{C\,(\cos^2\alpha + 1)\sin\alpha}{(kH)^2} \tag{2.8}$$

One can observe in figure 7 that this analysis gives the correct qualitative picture.

2.5. *Lubricated regime dominated by gravity induced pressure (regime $g_{(f)}$)*

As before, we consider the asymptotic regime where gravity induced pressure balances the slope effects ($\mathcal{F} \to 0$), leading to a flat free surface: $\Delta = -Z$. The conservation of

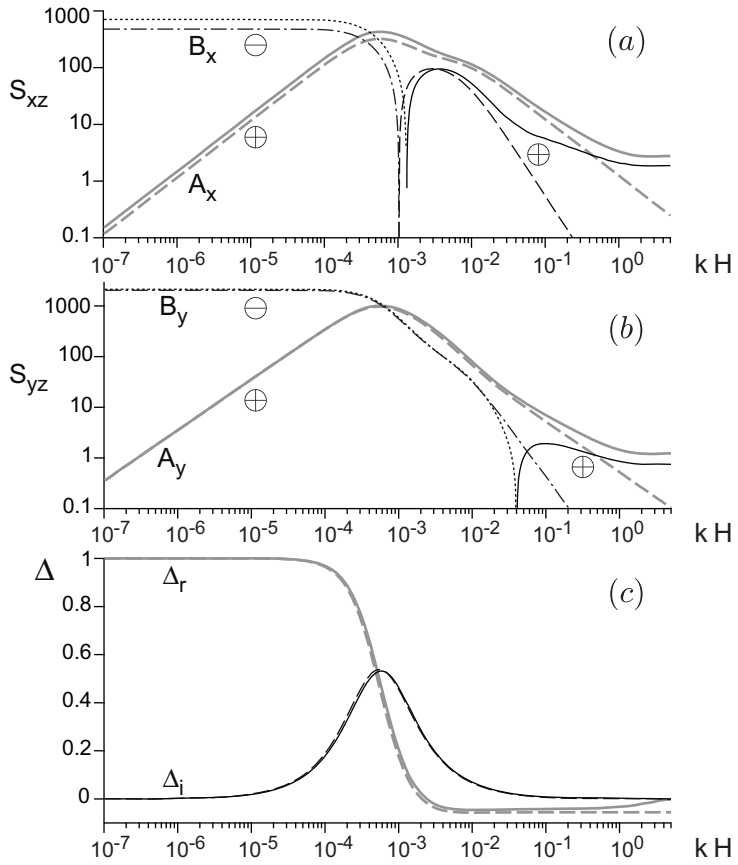

FIGURE 6. Comparison between the Reynolds averaged (solid and dotted lines) and Saint-Venant predictions (dashed and dotted lines) for the basal shear stresses and the free surface deformation, for $\alpha = 40^\circ$ and $\mathcal{F} = 0.3$. By convention, we have represented the absolute value of the quantities and indicated the sign by a $\oplus$ (solid and dashed lines) or a $\ominus$ (dotted or dotted-dashed lines). (a) A_x and B_x as functions of kH. (b) A_y and B_y as functions of kH. (c) Free surface deformation $\Delta = \Delta_r + i\Delta_i$.

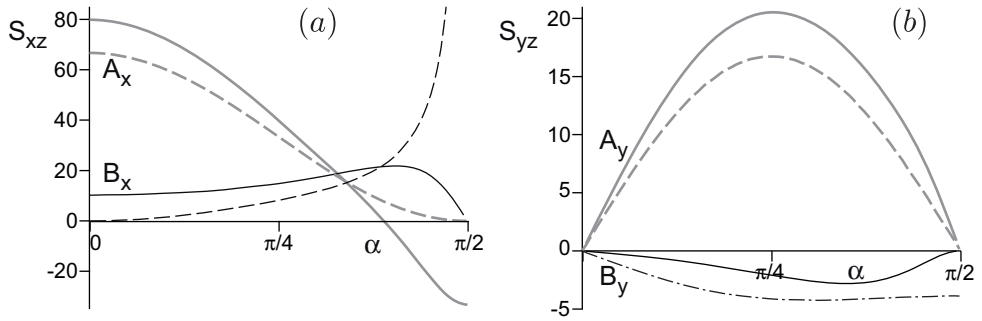

FIGURE 7. Basal shear stresses A_x, B_x, A_y, B_y as functions of α in the flat free surface regime, with inertia dominating friction (regime $g_{(i)}$). The parameters are $kH = 3\,10^{-2}$, $H/z_0 = 10^3$ and $\mathcal{F} = 0.1$.

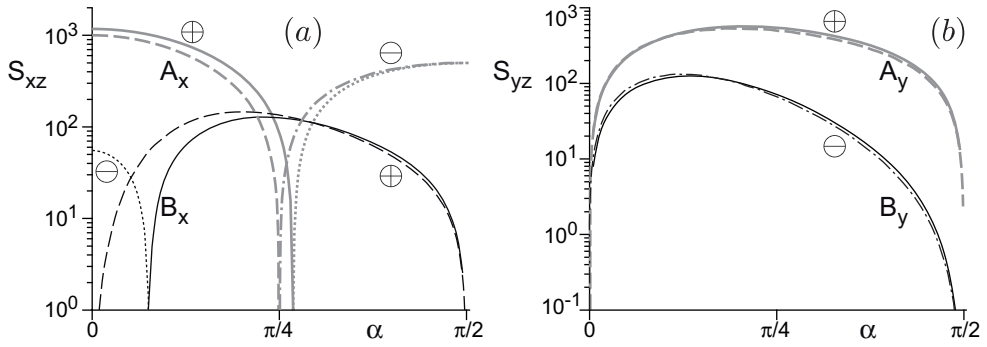

FIGURE 8. Basal shear stresses A_x, B_x, A_y, B_y as functions of α in the flat free surface regime, with friction dominating inertia (regime $g_{(f)}$). The parameters are $kH = 2\,10^{-3}$, $H/z_0 = 10^3$ and $\mathcal{F} = 0.1$.

mass then leads again to $u_\perp = \overline{u}\cos\alpha\,\frac{Z}{H}$. In the momentum balance along the direction parallel to the bedforms, we now consider that the turbulent friction is dominant and must vanish at the leading order:

$$(1+\sin^2\alpha)\,u_\parallel \sim \sin\alpha\cos\alpha u_\perp - \sin\alpha\frac{\Delta}{H}\overline{u} \sim \sin\alpha\left(\cos^2\alpha+1\right)\,\frac{Z}{H}\overline{u}. \tag{2.9}$$

This leads to:

$$A_x = \frac{2\,\cos(2\alpha)}{(1+\sin^2\alpha)\,kH} \quad \text{and} \quad A_y = \frac{3\sin(2\alpha)}{2(1+\sin^2\alpha)\,kH}\,. \tag{2.10}$$

We now reintroduce inertia at the perturbative order: the inertial term $ikH\,\cos\alpha\,u_\parallel$ is equal to

$$ikH\,\frac{\cos\alpha\,\sin\alpha\left(\cos^2\alpha+1\right)}{1+\sin^2\alpha}\,\frac{Z_1}{H}\overline{u} \tag{2.11}$$

at the leading order. It is balanced by turbulent friction term $-C(1+\sin^2\alpha)\,u_\parallel$. As before, this results into a positive B_x and a negative B_y:

$$B_x = \frac{2\cos\alpha\,\sin^2\alpha\,\left(1+\cos^2\alpha\right)}{C\left(1+\sin^2\alpha\right)^2} \quad \text{and} \quad B_y = -\frac{\cos^2\alpha\,\sin\alpha\,\left(1+\cos^2\alpha\right)}{C\left(1+\sin^2\alpha\right)^2}\,. \tag{2.12}$$

One can observe in figure 8 that the prediction of the Saint-Venant equations compares very well to the Reynolds averaged calculation, except for B_x in the neighbourhood of $\alpha = 0$.

2.6. *Lubricated regime dominated by friction (regime $f_{(g)}$)*

We finally consider the asymptotic regime in which both inertia and gravity induced pressure can be neglected, so that the downslope gravity component is balanced by turbulent friction. We call u_1 and v_1 the velocity disturbances respectively along the main flow direction and transverse to it. The transverse velocity follows the transverse slope:

$$v_1 = -\frac{i}{C\mathcal{F}^2}\,k\,\sin\alpha\,Z\,\overline{u}. \tag{2.13}$$

By conservation of mass, one gets:

$$\frac{\overline{u}}{H}\,\Delta + u_1 = -\tan\alpha\;v_1. \tag{2.14}$$

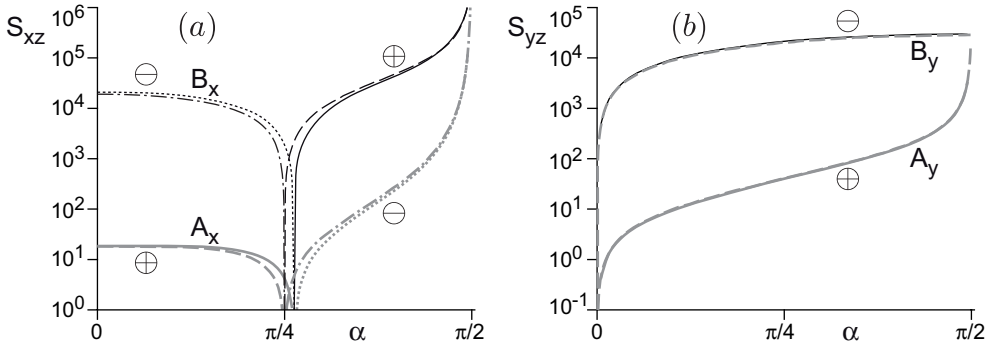

FIGURE 9. Basal shear stresses A_x, B_x, A_y, B_y as functions of α in the friction dominated regime (regime $f_{(g)}$). The parameters are $kH = 10^{-7}$, $H/z_0 = 10^3$ and $\mathcal{F} = 0.1$.

The longitudinal slope tends also to entrain the fluid downslope:

$$2u_1 - \frac{\overline{u}}{H}\,\Delta = -\frac{i}{C\mathcal{F}^2}\,k\,\cos\alpha\,Z\,\overline{u}. \tag{2.15}$$

One then obtains $A_x = A_y = 0$, and

$$B_x = \frac{2(\sin\alpha\tan\alpha - \cos\alpha)}{3C\mathcal{F}^2} \quad \text{and} \quad B_y = -\frac{\sin\alpha}{C\mathcal{F}^2}. \tag{2.16}$$

This regime is reached in the limit of vanishing kH. The sign of B_x is determined by two antagonist mechanisms. At small angle α, the dominant effect is that of the longitudinal slope, which leads longitudinally to a downslope fluid motion ($B_x < 0$). At large angle α, the dominant effect is that of the transverse slope which leads transversally to a downslope fluid motion ($B_y < 0$). However, through mass conservation, this leads to an upslope longitudinal fluid motion $B_x > 0$. When reintroducing the gravity-induced pressure at the perturbative order, one obtains:

$$A_x = \frac{2}{9C^2\mathcal{F}^4}\,\left[2 - \cos(2\alpha) - 2\tan^2\alpha\right]\,kH \quad \text{and} \quad A_y = \frac{1}{6C^2\mathcal{F}^4}\,[3 - \cos(2\alpha)]\tan\alpha\,kH. \tag{2.17}$$

One can observe in figure 8 that, in this regime, the prediction of the Saint-Venant equations almost perfectly fit the Reynolds averaged calculation.

2.7. *Regime diagram*

We can now come back to the regime diagram (Fig. 2). Friction dominates at vanishing kH while gravity-induced pressure dominates at larger values of kH. The cross-over between these regimes is associated to a transition of the flow thickness modulation from 0 to 1. At a vanishing bedform angle $\alpha = 0$, the Saint-Venant equations predict that this transition occurs at:

$$kH = \frac{3C\mathcal{F}^2}{1 - \mathcal{F}^2}\,. \tag{2.18}$$

It vanishes when the Froude approaches 0 and tends to infinity at $\mathcal{F} = 1$. At an angle α close to $\pi/2$, the transition wavenumber can be approximated into:

$$kH = \frac{3\sqrt{3}}{2}\,\left(\frac{\pi}{2} - \alpha\right)\,C\mathcal{F}^2. \tag{2.19}$$

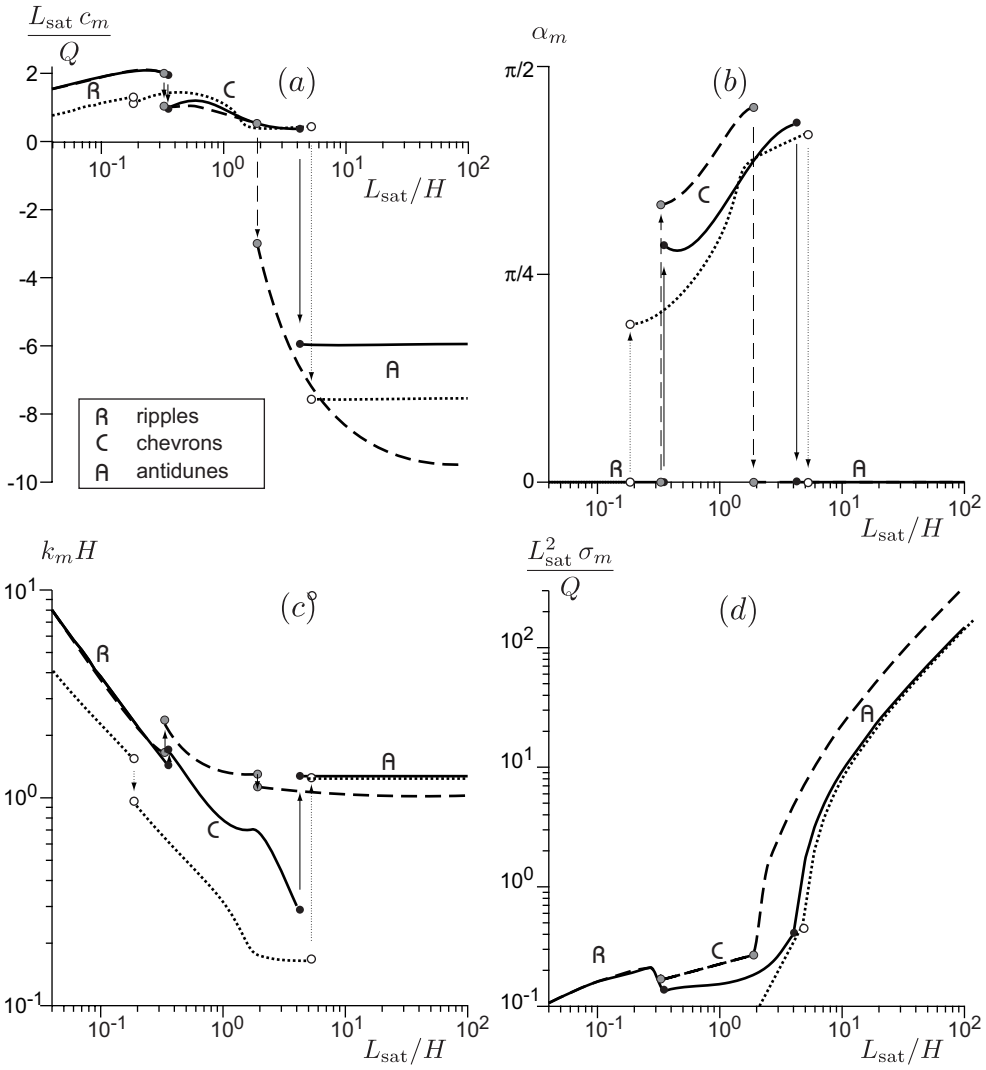

FIGURE 10. Characteristics of the most unstable mode as a function of $L_{\rm sat}/H$ for $\mathcal{F} = 1$: $u_*/u_{\rm th} \to 1$ and $\mu \to \infty$ (solid lines), $u_*/u_{\rm th} \to 1$ and $\mu = \tan(32°)$ (dashed lines) and $u_*/u_{\rm th} \to \infty$ wathever the value of μ (dotted line). H/z_0 is kept constant and equal to 10^2. (a) Propagation speed c_m. (b) Angle α_m of the wavenumber with respect to the flow direction. (c) Wavenumber k_m rescaled by the flow thickness. (d) Growth rate σ_m.

In the flat free surface regime, the transition between friction dominating inertia and inertia dominating friction occurs for:

$$kH = C\,\frac{1+\sin^2\alpha}{\cos\alpha} \tag{2.20}$$

At this wave-number, the asymptotic expansions of B_x and B_y determined previously coincide.

The shallow water approximation is valid when the inner layer invades the whole flow thickness. The cross-over with the regime in which an inner and an outer layers coexist

occurs for:

$$kH \simeq 40\, C \tag{2.21}$$

Finally, the resonance of standing surface waves occurs for $\mathcal{F} = 1/\cos\alpha$ at low kH and for $\mathcal{F} = 1/(\sqrt{kH}\,\cos\alpha)$ at large kH. These different transitions are reported in figure 2.

3. Influence of secondary parameters on the transition between ripples and antidunes

Supplementary figure 10 shows the dependence of the bifurcation diagram on two secondary parameters: $u_*/u_{\rm th}$ and the effective friction coefficient μ. One observes that they do not induce significant changes in the anti-dune regime.

REFERENCES

Fourrière, A., Claudin P. & Andreotti, B. 2010 Bedforms in a turbulent stream: formation of ripples by primary linear instability and of dunes by non-linear pattern coarsening. *J. Fluid Mech.* **649**, 287-328.

Jackson, P.S. & Hunt, J.C.R. 1975 Turbulent wind flow over a low hill. *Q. J. R. Meteorol. Soc.* **101**, 929.

Kroy, K., Sauermann, G. & Herrmann, H.J. 2002 Minimal model for aeolian sand dunes. *Phys. Rev. E* **66**, 031302.

Reynolds, O. 1874 On the extent and action of the heating surface of steam boilers. *Proc. Manchester Lit. Phil. Soc.* **8**.